Journal of Sound and Vibration 329 (2010) 3335–3347

Contents lists available at ScienceDirect

Journal of Sound and Vibration

journal homepage: www.elsevier.com/locate/jsvi

Uncertainty analysis near bifurcation of an aeroelastic system

M. Ghommem, M.R. Hajj *, A.H. Nayfeh

Department of Engineering Science and Mechanics, MC 0219, Virginia Polytechnic Institute and State University, Blacksburg, VA 24061, USA

ARTICLE INFO

Article history:
Received 14 October 2009
Received in revised form
26 February 2010
Accepted 26 February 2010
Handling Editor: L.N. Virgin
Available online 30 March 2010

ABSTRACT

Variations in structural and aerodynamic nonlinearities on the dynamic behavior of an aeroelastic system are investigated. The aeroelastic system consists of a rigid airfoil that is supported by nonlinear springs in the pitch and plunge directions and subjected to nonlinear aerodynamic loads. We follow two approaches to determine the effects of variations in the linear and nonlinear plunge and pitch stiffness coefficients of this aeroelastic system on its stability near the bifurcation. The first approach is based on implementation of intrusive polynomial chaos expansion (PCE) on the governing equations, yielding a set of nonlinear coupled ordinary differential equations that are numerically solved. The results show that this approach is capable of determining sensitivity of the flutter speed to variations in the linear pitch stiffness coefficient. On the other hand, it fails to predict changes in the type of the instability associated with randomness in the cubic stiffness coefficient. In the second approach, the normal form is used to investigate the flutter (Hopf bifurcation) boundary that occurs as the freestream velocity is increased and to analytically predict the amplitude and frequency of the ensuing LCO. The results show that this mathematical approach provides detailed aspects of the effects of the different system nonlinearities on its dynamic behavior. Furthermore, this approach could be effectively used to perform sensitivity analysis of the system's response to variations in its parameters.

1. Introduction

Uncertainties in linear and nonlinear parameters of any aeroelastic system impact its stability and response. A common system that has been used to investigate the aeroelastic behavior and dynamic instabilities is a two-dimensional rigid airfoil undergoing pitch and plunge motions [1,2]. Beran et al. [3] carried out an analysis to quantify the uncertain response of a rigid airfoil supported by nonlinear springs in the pitch and plunge directions. Uncertainties were specified in the cubic coefficient of the torsional spring and the initial pitch angle of the airfoil. They performed stochastic projections of the time-domain and cyclic equations governing the airfoil response. Wu et al. [4] investigated the effect of parameter uncertainties on the flutter characteristics of a two-dimensional airfoil in an incompressible flow through a Gegenbauer polynomial approximation. Their results showed that the randomness of the linear component of the spring affects the onset of flutter and the randomness of the cubic component of the spring affects the amplitude of the LCO. Millman et al. [5] used Fourier chaos expansions (FCE) to obtain probability distributions of the amplitudes of the pitch responses due to randomness in the initial pitch angle and the cubic stiffness coefficient of the pitch spring. They found that, unlike the

* Corresponding author. Tel.: +1 540 2314190; fax: +1 540 2314574.
E-mail address: mhajj@vt.edu (M.R. Hajj).

0022-460X/$ - see front matter © 2010 Elsevier Ltd. All rights reserved.
doi:10.1016/j.jsv.2010.02.028

polynomial chaos expansions (PCE), which fail to predict limit-cycle oscillations, the FCE can predict both subcritical and supercritical responses even with low-order expansions and higher-order nonlinearities.

Combined nonlinear (geometric, inertia, free-play, damping, and/or aerodynamics) aspects that contribute to unstable responses of any aeroelastic system could be either of the supercritical or subcritical type. In Fig. 1, we show a qualitative sketch of the system behavior. In the supercritical instability, the system response is stable to any disturbance below the flutter boundary. Beyond this boundary, nonlinearities yield LCO whose amplitude increases slowly with increasing flight speed. In the subcritical type, a sudden jump to a large-amplitude LCO takes place at or below the flutter speed, depending on the initial conditions. Uncertainties in the linear and nonlinear parameters may lower the flutter speed and lead to the undesirable subcritical behavior even if the deterministic design or solution exhibits supercritical behavior only. These effects are schematically illustrated by the arrows in Fig. 1. Uncertainties of the linear parameters would cause the deterministic supercritical behavior represented by curve **A** to follow curve $\mathbf{A}'$. Uncertainties in nonlinear parameters could cause the supercritical response represented by curve $\mathbf{A}'$ to become subcritical as represented by curve $\mathbf{A}''$. Depending on the initial conditions, the system's response could exhibit subcritical behavior at speeds that are much lower than the flutter speed predicted with the deterministic approach.

To deal with these uncertainties, a common approach is to assign probabilistic distributions to certain input variables and structural parameters and use uncertainty propagation methods (sampling approaches such as Monte Carlo simulations (MCs) and Latin hypercube sampling (LHS) and response surface approaches, such as PCE, FCE [6,7]) to obtain probability distributions functions (PDFs) of supercritical and subcritical responses. Following these approaches, one may obtain a range of variations of the LCO amplitude within a type of instability [5,8], as shown in Fig. 1. Since aeroelastic systems are usually not designed to operate beyond the flutter boundary, there is no need to quantify uncertain LCO in those regions. Under these conditions, modern methods of nonlinear dynamics may be effectively implemented and used to perform the analysis near the bifurcation and especially capture the switch from the supercritical to the subcritical instability.

In this work, we assess two approaches for determining the effects of variations in the linear and nonlinear spring coefficients of an aeroelastic system on its stability near a bifurcation point. In the first approach, we implement the intrusive PCE in the governing equations. This expansion yields a set of coupled equations that are numerically solved. In the second approach, we use modern methods of nonlinear dynamics to derive the normal form. A comparison of the usefulness and effectiveness of these approaches is shown by characterizing sensitivity of the response of the system to variations in its parameters.

2. Representation of the aeroelastic system

The aeroelastic system, considered in this work, is modeled as a rigid wing allowed to move with two degrees of freedom as presented in Fig. 2. The wing is free to rotate about the elastic axis (pitch motion) and translate vertically (plunge motion). Denoting by h and α the plunge deflection and pitch angle, respectively, one can write the governing

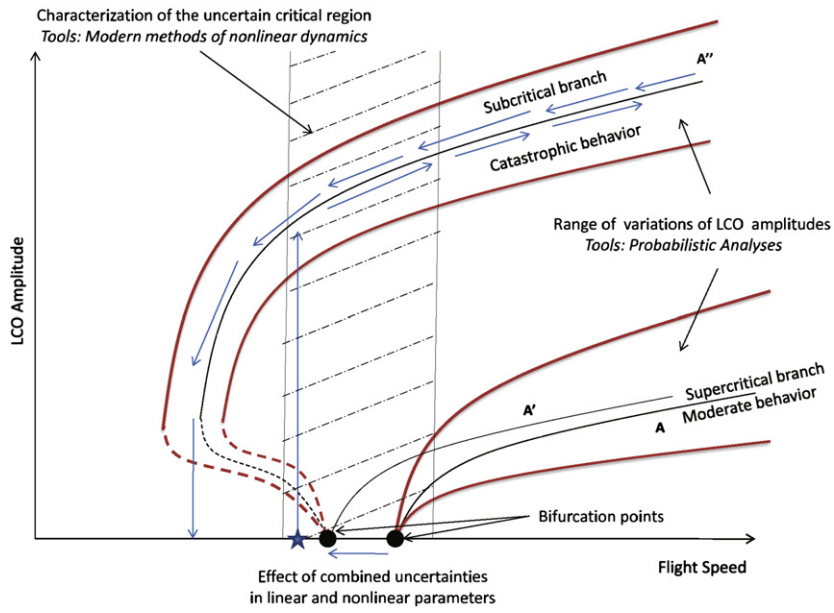

Fig. 1. Schematic of LCO response of an aeroelastic system. Arrows denote path of system response that may occur due to uncertainty in structural or aerodynamic parameters: (→) increasing, (←) decreasing.

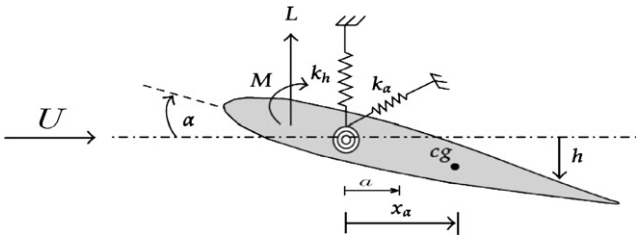

Fig. 2. Sketch of a two-dimensional airfoil.

equations of this system as [9,10]

$$\begin{pmatrix} m_T & m_W x_\alpha b \\ m_W x_\alpha b & I_\alpha \end{pmatrix} \begin{pmatrix} \ddot{h} \\ \ddot{\alpha} \end{pmatrix} + \begin{pmatrix} c_h & 0 \\ 0 & c_\alpha \end{pmatrix} \begin{pmatrix} \dot{h} \\ \dot{\alpha} \end{pmatrix} + \begin{pmatrix} k_h(h) & 0 \\ 0 & k_\alpha(\alpha) \end{pmatrix} \begin{pmatrix} h \\ \alpha \end{pmatrix} = \begin{pmatrix} -L \\ M \end{pmatrix} \tag{1}$$

where m_T is the total mass of the wing and its support structure; m_W is the wing mass alone; I_α is the mass moment of inertia about the elastic axis; b is half chord length; $x_\alpha = r_{cg}/b$ is the nondimensional distance between the center of mass and the elastic axis; c_h and c_α are the plunge and pitch viscous damping coefficients, respectively; L and M are the aerodynamic lift and moment about the elastic axis, and k_h and k_α are the structural stiffness for the plunge and pitch motions, respectively. The representative parameters of this stiffness are approximated in polynomial form by

$$k_\alpha(\alpha) = k_{\alpha 0} + k_{\alpha 1}\alpha + k_{\alpha 2}\alpha^2 + \cdots$$

$$k_h(h) = k_{h0} + k_{h1}h + k_{h2}h^2 + \cdots \tag{2}$$

The aerodynamic loads are evaluated using a quasi-steady approximation with a stall model [10] and written as

$$L = \rho U^2 b c_{l_\alpha}(\alpha_{\text{eff}} - c_s \alpha_{\text{eff}}^3)$$

$$M = \rho U^2 b^2 c_{m_\alpha}(\alpha_{\text{eff}} - c_s \alpha_{\text{eff}}^3) \tag{3}$$

where U is the freestream velocity, c_{l_α} and c_{m_α} are the aerodynamic lift and moment coefficients, and c_s is a nonlinear parameter associated with stall. The effective angle of attack due to the instantaneous motion of the airfoil is given by [10]

$$\alpha_{\text{eff}} = \left[\alpha + \frac{\dot{h}}{U} + \left(\frac{1}{2} - a\right) b \frac{\dot{\alpha}}{U}\right] \tag{4}$$

where a is the nondimensional distance from the midchord to the elastic axis.

For the sake of subsequent analyses, we define the state variables

$$\mathbf{Y} = \begin{pmatrix} Y_1 \\ Y_2 \\ Y_3 \\ Y_4 \end{pmatrix} = \begin{pmatrix} h \\ \alpha \\ \dot{h} \\ \dot{\alpha} \end{pmatrix}$$

and write the equations of motion in the form

$$\dot{\mathbf{Y}} = F(\mathbf{Y}, U), \tag{5}$$

where

$$F(\mathbf{Y},U) = \begin{pmatrix} Y_3 \\ Y_4 \\ -p_h(Y_1)Y_1 - (k_1 U^2 + p_\alpha(Y_2))Y_2 - c_1 Y_3 - c_2 Y_4 + g_{NL1}(Y) \\ -q_h(Y_1)Y_1 - (k_2 U^2 + q_\alpha(Y_2))Y_2 - c_3 Y_3 - c_4 Y_4 + g_{NL2}(Y) \end{pmatrix} \tag{6}$$

The relations of the new variables used in Eq. (6) to the physical parameters are provided in Table 1. The original system, Eq. (5), is then rewritten as

$$\dot{\mathbf{Y}} = A(U)\mathbf{Y} + Q(\mathbf{Y},\mathbf{Y}) + C(\mathbf{Y},\mathbf{Y},\mathbf{Y}) \tag{7}$$

where $Q(\mathbf{Y},\mathbf{Y})$ and $C(\mathbf{Y},\mathbf{Y},\mathbf{Y})$ are, respectively, the quadratic and cubic vector functions of the state variables collected in the vector $\mathbf{Y}$.

To determine the system's stability, we consider the linearized governing equations, which are written in a first-order differential form as

$$\dot{\mathbf{Y}} = A(U)\mathbf{Y} \tag{8}$$

Table 1
System variables.

$d = m_T I_\alpha - m_W^2 x_\alpha^2 b^2$
$k_1 = (I_\alpha \rho b c_{l_\alpha} + m_W x_\alpha \rho b^3 c_{m_\alpha})/d$
$k_2 = -(m_W x_\alpha \rho b^2 c_{l_\alpha} + m_T \rho b^2 c_{m_\alpha})/d$
$c_1 = [I_\alpha (c_h + \rho U b c_{l_\alpha}) + m_W x_\alpha \rho U b^3 c_{m_\alpha}]/d$
$c_2 = [I_\alpha \rho U b^2 c_{l_\alpha} (\frac{1}{2} - a) - m_W x_\alpha b c_{l_\alpha} + m_W x_\alpha \rho U b^4 c_{m_\alpha} (\frac{1}{2} - a)]/d$
$c_3 = [-m_W x_\alpha b (c_h + \rho U b c_{l_\alpha}) - m_T x_\alpha \rho U b^2 c_{m_\alpha}]/d$
$c_4 = [m_T (c_\alpha - \rho U b^3 c_{m_\alpha} (\frac{1}{2} - a)) - m_W x_\alpha \rho U b^3 c_{l_\alpha} (\frac{1}{2} - a)]/d$
$p_\alpha(\mathbf{Y}) = -m_W x_\alpha b k_\alpha(\mathbf{Y})/d$
$q_\alpha(\mathbf{Y}) = m_T k_\alpha(\mathbf{Y})/d$
$p_h(\mathbf{Y}) = I_\alpha k_h(\mathbf{Y})/d$
$q_h(\mathbf{Y}) = -m_W x_\alpha b k_h(\mathbf{Y})/d$
$g_{NL1}(\mathbf{Y}) = (c_s \rho U^2 b)(c_{l_\alpha} I_\alpha + m_W x_\alpha b^2 c_{m_\alpha}) \alpha_{\text{eff}}^3(\mathbf{Y})/d$
$g_{NL2}(\mathbf{Y}) = -(c_s \rho U^2 b^2)(c_{l_\alpha} m_W x_\alpha + m_T c_{m_\alpha}) \alpha_{\text{eff}}^3(\mathbf{Y})/d$

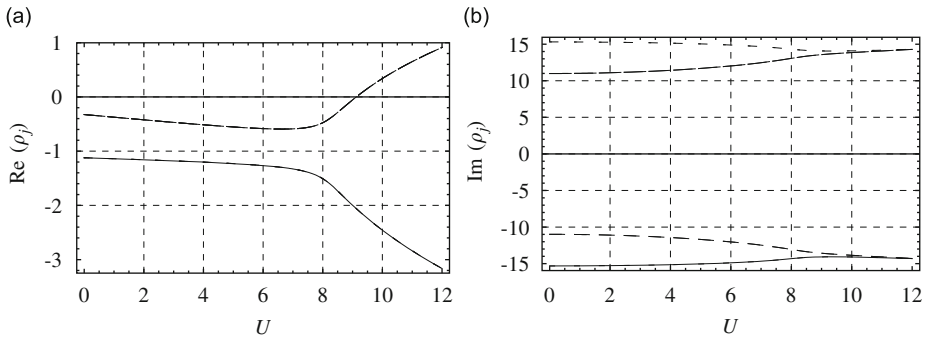

Fig. 3. Variations of (a) the real (damping) and (b) imaginary (frequency) parts of the ρ_j with the freestream velocity U (m/s).

where

$$A(U) = \begin{pmatrix} 0 & 0 & 1 & 0 \\ 0 & 0 & 0 & 1 \\ -I_\alpha k_{h0}/d & -(k_1 U^2 - m_W x_\alpha b k_{\alpha 0}/d) & -c_1 & -c_2 \\ m_W x_\alpha b k_{h0}/d & -(k_2 U^2 + m_T k_{\alpha 0}/d) & -c_3 & -c_4 \end{pmatrix} \tag{9}$$

The 4×4 matrix $A(U)$ has a set of four eigenvalues, $\{\rho_j, j = 1,2,\ldots,4\}$. These eigenvalues determine the stability of the trivial solution of Eq. (8). If the real parts of all of the ρ_j are negative, the trivial solution is asymptotically stable. On the other hand, if the real part of one or more eigenvalues are positive, the trivial solution is unstable. The flutter speed U_f, for which one or more eigenvalues have zero real parts, corresponds to the onset of linear instability. For the specific values given in Strganac et al. [10], Figs. 3(a) and (b) show, respectively, variations of the real and imaginary parts of the ρ_j with U. It is noted that two of the eigenvalues transversally cross the imaginary axis at U_f=9.1242 m/s. At this speed, the aeroelastic system undergoes a Hopf bifurcation as indicated by the oscillatory solution ($\text{Im}(\rho) \neq 0$). The observed coalescence of the two aeroelastic modal frequencies is indicative of classical flutter.

3. Uncertainty quantification via intrusive polynomial chaos

In this section, we implement the intrusive formulation of the polynomial chaos expansion (PCE) to quantify uncertainty in the flutter speed and the LCO of the aeroelastic system described above due to imprecision in the pitch stiffness. This formulation involves substitution of uncertain variables and parameters in the governing equations with polynomial expansions. The unknowns polynomial coefficients are then evaluated by projecting the resulting equations onto basis functions. Thus, the governing equations are reformulated to yield mode strengths [11] of the output.

We consider variations in the linear and cubic pitch stiffness coefficients $k_{\alpha 0}$ and $k_{\alpha 2}$ described by Gaussian distributions and expressed in the following standard forms:

$$k_{\alpha 0} = \overline{k}_{\alpha 0} + \sigma_1 \xi_1 \tag{10}$$

$$k_{\alpha 2} = \overline{k}_{\alpha 2} + \sigma_2 \xi_2 \tag{11}$$

The effects of randomness in these parameters on the speed at flutter onset of the airfoil and ensuing LCO amplitudes are determined by numerically integrating the set of governing equations. In general, the linear and cubic stiffness coefficients may not vary independently. Yet, the flutter speed would only be impacted by the variations in the linear coefficient. On the other hand, the LCO amplitude would be impacted by variations in both coefficients. These effects will be made clear from the normal form derivation presented in Section 4. For physical evaluation of the randomness effects of each parameter, we treat them separately.

3.1. Effect of randomness of $k_{\alpha 0}$ on the flutter speed

In implementing the intrusive approach, the plunge displacement h and pitch angle α are considered as stochastic processes that are functions of the uncertain parameters. Their PCEs are then written as

$$h(t,\xi_1)=\sum_{i=0}^{P} h_i(t)\Psi_i(\xi_1)$$

$$\alpha(t,\xi_1)=\sum_{i=0}^{P} \alpha_i(t)\Psi_i(\xi_1) \tag{12}$$

where $P+1=(n+p)!/n!p!$ is the number of output modes, which is a function of the order of the polynomial chaos p and the number of random dimensions n. Here, the $h_i(t)$ and $\alpha_i(t)$ are the deterministic components, the amplitudes of the plunge and pitch fluctuation, respectively, and $\Psi_i(\xi_1)$ is the random basis function corresponding to the i th mode. Many choices are possible for the basis functions, depending on the type of the probability distribution selected for the uncertainty of the random variable vector ξ_1 [12]. For variables with Gaussian probability distributions, Hermite polynomials are used because they form an orthogonal set of basis functions [13]. Taking p=1 (i.e., keep only the linear terms) and substituting Eqs. (10) and (12) into Eq. (8), we have

$$\dot{\mathbf{Y}}=\begin{pmatrix} 0 & 0 & 1 & 0 \\ 0 & 0 & 0 & 1 \\ -I_\alpha k_{h0}/d & -(k_1U^2-m_W x_\alpha b(\overline{k}_{\alpha 0}+\sigma_1\xi_1)/d) & -c_1 & -c_2 \\ m_W x_\alpha b k_{h0}/d & -(k_2U^2+m_T(\overline{k}_{\alpha 0}+\sigma_1\xi_1)/d) & -c_3 & -c_4 \end{pmatrix}\mathbf{Y} \tag{13}$$

where

$$\mathbf{Y}=\begin{pmatrix} h_0(t)+h_1(t)\xi_1 \\ \alpha_0(t)+\alpha_1(t)\xi_1 \\ \dot{h}_0(t)+\dot{h}_1(t)\xi_1 \\ \dot{\alpha}_0(t)+\dot{\alpha}_1(t)\xi_1 \end{pmatrix}$$

Multiplying both sides of Eq. (13) by $\Psi_i(\xi_1)$, i=0,1 in sequence, using the orthogonality of the basis functions (Hermite polynomials), and taking the inner product with respect to the random variable, we obtain

$$\dot{Y}_s=A_s(U)Y_s \tag{14}$$

where

$$Y_s=(h_0\ \ \alpha_0\ \ \dot{h}_0\ \ \dot{\alpha}_0\ \ h_1\ \ \alpha_1\ \ \dot{h}_1\ \ \dot{\alpha}_1)^T$$

$$A_s(U)=\begin{pmatrix} A(U) & D(\sigma_1) \\ D(\sigma_1) & A(U) \end{pmatrix} \tag{15}$$

and

$$D(\sigma_1)=\begin{pmatrix} 0 & 0 & 0 & 0 \\ 0 & 0 & 0 & 0 \\ 0 & m_W x_\alpha b\sigma_1/d & 0 & 0 \\ 0 & -m_T\sigma_1/d & 0 & 0 \end{pmatrix} \tag{16}$$

The matrix $A_s(U)$ has a set of eigenvalues, $\{\rho_j j=1,2,\ldots,8\}$, which determine the stability of the system given by Eq. (14). It is well-known that if the real parts of all ρ_j are negative, then the obtained solution is asymptotically stable. On the other hand, if one or more real parts of ρ_j are greater than zero, the solution is unstable. The flutter onset speed U_f is reached when one or more eigenvalues cross the imaginary axis into the right-half of the complex plane.

Fig. 4 shows variation of the real parts of the ρ_j with the freestream velocity U. It shows the ranges of the onset flutter speed of the stochastic airfoil system for different values of σ_1. Fig. 5 depicts variations of the upper U_{fu} and lower U_{fl} bounds of the flutter speed with σ_1 using both exact and PCE solutions. Clearly, as σ_1 increases, there is a slight departure

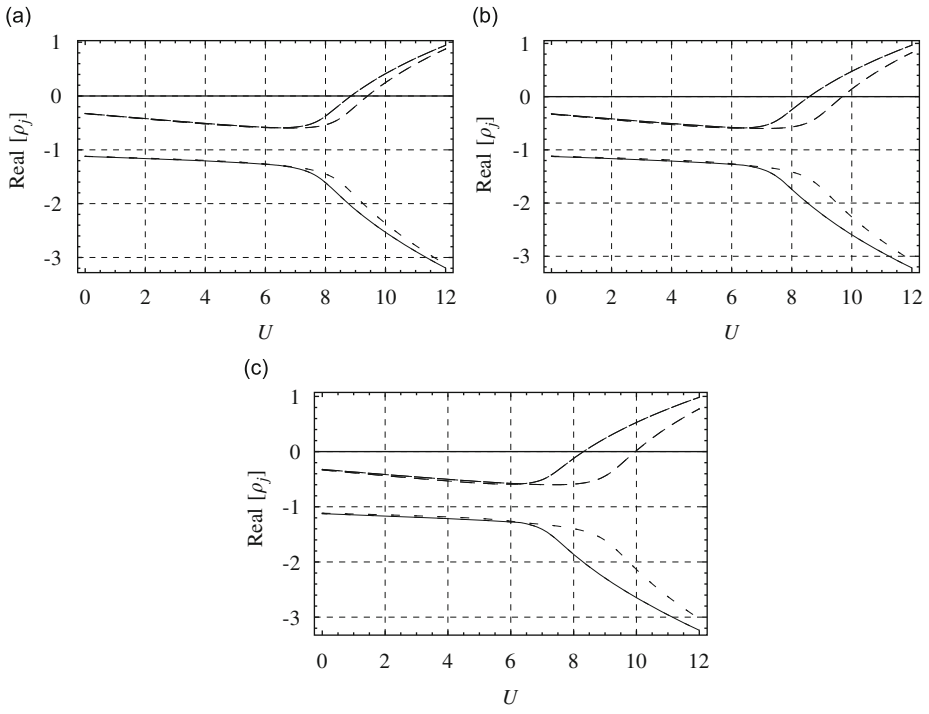

Fig. 4. Variation of the real part of ρ_j with the freestream velocity U (m/s). (a) $\sigma_1 = 0.05\overline{k}_{\alpha 0}$ (U_{fl}=8.84929, U_{fu}=9.40177), (b) $\sigma_1 = 0.1\overline{k}_{\alpha 0}$ (U_{fl}=8.57824, U_{fu}=9.68138), and (c) $\sigma_1 = 0.15\overline{k}_{\alpha 0}$ (U_{fl}=8.31217, U_{fu}=9.96227).

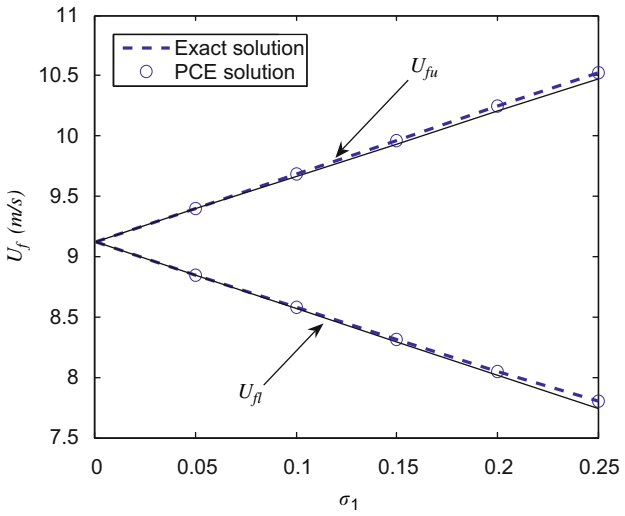

Fig. 5. Variation of flutter onset speed U_f (m/s) with σ_1. The solid line passes through the first two points and is drawn to show the departure from linear variations with σ_1.

from linear variations. However, a comparison between the exact flutter speeds and corresponding ones obtained from PCE-based analysis shows that the first-order intrusive PCE produces coefficients that accurately yield the sensitivity of the flutter speed to variations in the structural stiffness.

3.2. *Effect of randomness of $k_{\alpha 2}$ on LCO*

In this case, the full nonlinear system is considered. For the sake of simplicity, we consider the case in which structural nonlinearity is applied only in the pitch degree of freedom; that is, k_{h1}=0, k_{h2}=0, c_s=0, $\overline{k}_{\alpha 1} = 39.996\,\mathrm{N\,m}$, and $\overline{k}_{\alpha 2} = 67.685\,\mathrm{N\,m}$. These values were selected to obtain a configuration that yields a supercritical instability. We consider

$k_{\alpha 2}$ as a random variable and $k_{\alpha 0}$ as deterministic (i.e., $\sigma_1 = 0$). Here, h and α are approximated by the following PCEs in terms of ξ_2:

$$h(t,\xi_2) = \sum_{i=0}^{P} h_i(t)\Psi_i(\xi_2)$$

$$\alpha(t,\xi_2) = \sum_{i=0}^{P} \alpha_i(t)\Psi_i(\xi_2) \tag{17}$$

The intrusive approach relies on a Galerkin-projection reformulation of the original model equations to arrive at governing equations for the strengths of PC modes of the model output. The governing equations are rewritten by substituting Eqs. (11) and (17) into Eq. (5); the result is

$$\sum_{i=0}^{P} \ddot{h}_i(t)\Psi_i(\xi_2) = -(I_\alpha k_{h0}/d)\sum_{i=0}^{P} h_i(t)\Psi_i(\xi_2) - \left[k_1U^2 - m_W x_\alpha b\left(k_{\alpha 0} + k_{\alpha 1}\sum_{i=0}^{P}\alpha_i(t)\Psi_i(\xi_2) + (\overline{k}_{\alpha 2} + \sigma_2\xi_2)\left(\sum_{i=0}^{N}\alpha_i(t)\Psi_i(\xi_2)\right)^2\right)\Big/ d\right]\sum_{i=0}^{P}\alpha_i(t)\Psi_i(\xi_2) - c_1\sum_{i=0}^{P}\dot{h}_i(t)\Psi_i(\xi_2) - c_2\sum_{i=0}^{P}\dot{\alpha}_i(t)\Psi_i(\xi_2) \tag{18}$$

$$\sum_{i=0}^{P} \ddot{\alpha}_i(t)\Psi_i(\xi_2) = (m_W x_\alpha b k_{h0}/d)\sum_{i=0}^{P} h_i(t)\Psi_i(\xi_2) - \left[k_2U^2 + m_T\left(k_{\alpha 0} + k_{\alpha 1}\sum_{i=0}^{P}\alpha_i(t)\Psi_i(\xi_2) + (\overline{k}_{\alpha 2} + \sigma_2\xi_2)\left(\sum_{i=0}^{P}\alpha_i(t)\Psi_i(\xi_2)\right)^2\right)\Big/ d\right]\sum_{i=0}^{P}\alpha_i(t)\Psi_i(\xi_2) - c_3\sum_{i=0}^{P}\dot{h}_i(t)\Psi_i(\xi_2) - c_4\sum_{i=0}^{P}\dot{\alpha}_i(t)\Psi_i(\xi_2) \tag{19}$$

Using the orthogonality of the basis functions (Hermite polynomials) and projecting Eqs. (18) and (19) onto the $\Psi_l(\xi_2)$ yields the following stochastic version of the aeroelastic model:

$$\ddot{h}_l(t) = -(I_\alpha k_{h0}/d)h_l(t) - (k_1U^2 - m_W x_\alpha b k_{\alpha 0}/d)\alpha_l(t) - c_1\dot{h}_l(t) - c_2\dot{\alpha}_l(t) + (m_W x_\alpha b k_{\alpha 1}/d)\sum_{i=0}^{P}\sum_{j=0}^{P}\zeta_{ijl}\alpha_i(t)\alpha_j(t) + (m_W x_\alpha b/d)\left(\sum_{i=0}^{P}\sum_{j=0}^{P}\sum_{k=0}^{P}\alpha_i(t)\alpha_j(t)\alpha_k(t)(\overline{k}_{\alpha 2}\varsigma_{ijkl} + \sigma_2\tau_{ijkl})\right) \tag{20}$$

$$\ddot{\alpha}_l(t) = (m_W x_\alpha b k_{h0}/d)h_l(t) - (k_2U^2 + m_T/d)\alpha_l(t) - c_3\dot{h}_l(t) - c_4\dot{\alpha}_l(t) - (m_T k_{\alpha 1}/d)\sum_{i=0}^{P}\sum_{j=0}^{P}\zeta_{ijl}\alpha_i(t)\alpha_j(t) - (m_T/d)\left(\sum_{i=0}^{P}\sum_{j=0}^{P}\sum_{k=0}^{P}\alpha_i(t)\alpha_j(t)\alpha_k(t)(\overline{k}_{\alpha 2}\varsigma_{ijkl} + \sigma_2\tau_{ijkl})\right) \tag{21}$$

where

$$\zeta_{ijl} = \langle \Psi_i(\xi_2)\Psi_j(\xi_2), \Psi_l(\xi_2)\rangle, \quad \varsigma_{ijkl} = \langle \Psi_i(\xi_2)\Psi_j(\xi_2)\Psi_k(\xi_2), \Psi_l(\xi_2)\rangle$$

$$\tau_{ijkl} = \langle \Psi_i(\xi_2)\Psi_j(\xi_2)\Psi_k(\xi_2)\xi_2, \Psi_l(\xi_2)\rangle \tag{22}$$

and $\langle,\rangle$ denotes the inner product with the standard Gaussian distribution as a weighting function.

The PCE coefficients $h_l(t)$ and $\alpha_l(t)$ (l=0,1,…,P) can be then determined by numerical integration of the obtained set of nonlinear coupled ordinary-differential equations. The PCE coefficients directly yield estimates of the mean value and the variance. Furthermore, the first-order terms in these coefficients provide a measure of the sensitivity of the stochastic response to each of the uncertain parameters.

We consider a first-order PCE (i.e, p=1) and plot in Fig. 6 the time histories of the pitch motion obtained from the deterministic model as well as from the stochastic one at U=9.8 m/s for different variations of the uncertain parameter $k_{\alpha 2}$. By integrating the dynamical system given by Eqs. (20) and (21), we observe that the LCO response diverges from the physical limit cycle (obtained from the deterministic model) to a spurious limit cycle. We also note that the solution would still drift to a nonphysical limit cycle even if the order of the PCE is increased. This is due to the global nature of the basis functions in the PCE [5,14]. As a matter of fact, Pettit and Beran [14] showed that PCE based on non-global basis functions could capture limit cycles of nonlinear aeroelastic systems. In Fig. 6(b), a large variation of $k_{\alpha 2}$ is considered ($\xi_2 = 5$) to check if the PCE is capable of capturing the switch from the supercritical instability to the subcritical one as would be detected using the normal form (see next section). It can be clearly seen that even for short-time integration, the PCE fails to predict the LCO for large variations of the uncertain cubic coefficient $k_{\alpha 2}$ of the pitch stiffness. Moreover, it cannot predict changes in the type of the instability. The intrusive formulation of the PCE shows weaknesses and lack of robustness in the modeling of stochastic oscillating aeroelastic systems characteristics.

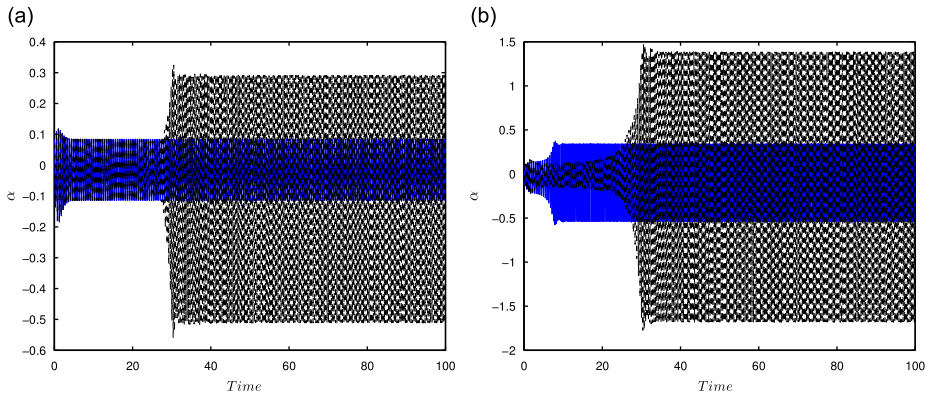

Fig. 6. Time histories of the pitch motion. The solid line represents the time history obtained by integrating numerically the deterministic model. The dashed line is from the stochastic model based on the first-order PCE. (a) $\xi_2 = 1$ and $\sigma_2 = 0.1\overline{k}_{\alpha 2}$ and (b) $\xi_2 = 5$ and $\sigma_2 = 0.1\overline{k}_{\alpha 2}$.

4. Uncertainty quantification via normal form of Hopf bifurcation

In this section, we follow a second approach, namely the normal form, to determine stochastic aspects of the response of aeroelastic systems as caused by variations in the system's parameters. To compute the normal form of the Hopf bifurcation of Eq. (7) near $U=U_f$, we follow Nayfeh and Balachandran [15] and introduce a small nondimensional parameter ε as a bookkeeping parameter and seek a third-order approximate solution of Eq. (7) in the form:

$$\mathbf{Y}(t) = \varepsilon \mathbf{Y}_1(T_0,T_2) + \varepsilon^2 \mathbf{Y}_2(T_0,T_2) + \varepsilon^3 \mathbf{Y}_3(T_0,T_2) + \cdots \tag{23}$$

where the time scales $T_m = \varepsilon^m t$. As shown below, the secular terms, arising from the nonlinear terms, appear at the third order and hence would have no dependence on the time scale T_1. Moreover, we set $U = U_f + \varepsilon^2 \sigma_U U_f$, $k_{\alpha 0} = \overline{k}_{\alpha 0} + \varepsilon^2 \sigma_\alpha \overline{k}_{\alpha 0}$, and $k_{h0} = \overline{k}_{h0} + \varepsilon^2 \sigma_h \overline{k}_{h0}$. These detunings are assumed to be of order $O(\varepsilon^2)$, again because the secular terms appear at order $O(\varepsilon^3)$.

The time derivative is expressed in terms of these scales as

$$\frac{\mathrm{d}}{\mathrm{d}t} = D_0 + \varepsilon^2 D_2 + \cdots \tag{24}$$

where $D_m = \partial/\partial T_m$. Substituting Eqs. (23) and (24) into Eq. (7) and equating coefficients of like powers of ε, we obtain

Order (ε):

$$D_0 \mathbf{Y}_1 - A(U_f)\mathbf{Y}_1 = 0 \tag{25}$$

Order (ε^2):

$$D_0 \mathbf{Y}_2 - A(U_f)\mathbf{Y}_2 = Q(\mathbf{Y}_1,\mathbf{Y}_1) \tag{26}$$

Order (ε^3):

$$D_0 \mathbf{Y}_3 - A(U_f)\mathbf{Y}_3 = -D_2 \mathbf{Y}_1 + \sigma_U B_1 \mathbf{Y}_1 + \sigma_h B_2 \mathbf{Y}_1 + \sigma_\alpha B_3 \mathbf{Y}_1 + 2Q(\mathbf{Y}_1,\mathbf{Y}_2) + C(\mathbf{Y}_1,\mathbf{Y}_1,\mathbf{Y}_1) \tag{27}$$

where

$$B_1 = -2U_f^2(k_1 I_1 + k_2 I_2), \quad B_2 = -\frac{I_\alpha}{\mathrm{d}} I_1 + \frac{m_W b x_\alpha}{\mathrm{d}} I_2,$$

$$B_3 = \frac{m_W b x_\alpha}{\mathrm{d}} I_1 - \frac{m_T}{\mathrm{d}} I_2, \quad I_1 = \begin{pmatrix} 0 & 0 & 0 & 0 \\ 0 & 0 & 0 & 0 \\ 0 & 1 & 0 & 0 \\ 0 & 0 & 0 & 0 \end{pmatrix}, \quad I_2 = \begin{pmatrix} 0 & 0 & 0 & 0 \\ 0 & 0 & 0 & 0 \\ 0 & 0 & 0 & 0 \\ 0 & 1 & 0 & 0 \end{pmatrix} \tag{28}$$

The general solution of Eq. (25) is the superposition of four linearly independent solutions corresponding to the four eigenvalues: two of these eigenvalues have negative real parts and the other two are purely imaginary ($\pm \mathrm{i}\omega$). Because the two solutions corresponding to the two eigenvalues with negative real parts decay as $T_0 \to \infty$, we retain only the nondecaying solutions and express the general solution of the first-order problem as

$$\mathbf{Y}_1(T_0,T_2) = \eta(T_2)\mathbf{p}\mathrm{e}^{\mathrm{i}\omega T_0} + \overline{\eta}(T_2)\overline{\mathbf{p}}\mathrm{e}^{-\mathrm{i}\omega T_0} \tag{29}$$

where $\eta(T_2)$ is determined by imposing the solvability condition [16] at the third-order level and $\mathbf{p}$ is the eigenvector of $A(U_f)$ corresponding to the eigenvalue $\mathrm{i}\omega$; that is,

$$A(U_f)\mathbf{p} = \mathrm{i}\omega\mathbf{p} \tag{30}$$

Substituting Eq. (29) into Eq. (26) yields

$$D_0\mathbf{Y}_2 - A(U_f)\mathbf{Y}_2 = Q(\mathbf{p},\mathbf{p})\eta^2 \mathrm{e}^{2\mathrm{i}\omega T_0} + 2Q(\mathbf{p},\overline{\mathbf{p}})\eta\overline{\eta} + Q(\overline{\mathbf{p}},\overline{\mathbf{p}})\overline{\eta}^2 \mathrm{e}^{-2\mathrm{i}\omega T_0} \tag{31}$$

The solution of Eq. (31) can be written as

$$\mathbf{Y}_2 = \zeta_2\eta^2 \mathrm{e}^{2\mathrm{i}\omega T_0} + 2\zeta_0\eta\overline{\eta} + \overline{\zeta}_2\overline{\eta}^2 \mathrm{e}^{-2\mathrm{i}\omega T_0} \tag{32}$$

where

$$[2\mathrm{i}\omega I - A(U_f)]\zeta_2 = Q(\mathbf{p},\mathbf{p}) \quad \text{and} \quad A(U_f)\zeta_0 = -Q(\mathbf{p},\overline{\mathbf{p}}) \tag{33}$$

Substituting Eqs. (29) and (32) into Eq. (27), we obtain

$$D_0\mathbf{Y}_3 - A(U_f)\mathbf{Y}_3 = -[D_2\eta\mathbf{p} - \sigma_U B_1\eta\mathbf{p} - \sigma_h B_2\eta\mathbf{p} - \sigma_\alpha B_3\eta\mathbf{p} - (4Q(\mathbf{p},\zeta_0) + 2Q(\overline{\mathbf{p}},\zeta_2) - 3C(\mathbf{p},\mathbf{p},\overline{\mathbf{p}}))\eta^2\overline{\eta}]\mathrm{e}^{\mathrm{i}\omega T_0} + cc + NST \tag{34}$$

where *cc* stands for the complex conjugate of the preceding terms and *NST* stands for terms that do not produce secular terms. We note that the homogeneous part of Eq. (34) is the same as Eq. (25) and that the latter has nontrivial solutions. Therefore, the nonhomogeneous Eq. (34) has a solution only if a solvability condition is satisfied. To determine this solvability condition, we define $\mathbf{q}$ as the left eigenvector of $A(U_f)$ corresponding to the eigenvalue $\mathrm{i}\omega$; that is,

$$A(U_f)^T\mathbf{q} = \mathrm{i}\omega\mathbf{q}$$

and normalize it so that $\mathbf{q}^T\mathbf{p}=1$. Then, the solvability condition requires that terms proportional to $\mathrm{e}^{\mathrm{i}\omega T_0}$ in Eq. (34) be orthogonal to $\mathbf{q}$. Imposing this condition, we obtain the following complex-valued normal form of the Hopf bifurcation:

$$\begin{aligned} D_2\eta = {} & [(0.434+0.324\mathrm{i})\sigma_U U_f - (4.135-1.502\mathrm{i})\sigma_h\overline{k}_{h0} + (2.398+4.011\mathrm{i})\sigma_\alpha\overline{k}_{\alpha 0}]\eta + [(0.559+0.936\mathrm{i}) \\ & \times 10^{-2}k_{\alpha 2} - (0.725+1.192\mathrm{i}) \times 10^{-3}k_{\alpha 1}^2 - (0.830+1.389\mathrm{i}) \times 10^{-3}k_{h1}k_{\alpha 1} - (2.199-0.798\mathrm{i}) \\ & \times 10^{-7}k_{h2} - (1.045-0.380\mathrm{i}) \times 10^{-7}k_{h1}^2 - (0.078+0.137\mathrm{i})c_s]\eta^2\overline{\eta} \end{aligned} \tag{35}$$

The effects of all nonlinearities, including the higher-order spring coefficients (k_{h1}, k_{h2}, $k_{\alpha 1}$, and $k_{\alpha 2}$) and aerodynamic parameter c_s, are explicitly expressed through the last six terms of this normal form. For convenience, we write Eq. (35) as

$$D_2\eta = \beta\eta + \Lambda\eta^2\overline{\eta} \tag{36}$$

where

$$\mathrm{Re}(\beta) = \beta_r = 0.434\sigma_U U_f - 4.135\sigma_h\overline{k}_{h0} + 2.398\sigma_\alpha\overline{k}_{\alpha 0}$$

$$\mathrm{Im}(\beta) = \beta_i = 0.324\sigma_U U_f + 1.502\sigma_h\overline{k}_{h0} + 4.011\sigma_\alpha\overline{k}_{\alpha 0}$$

$$\mathrm{Re}(\Lambda) = \Lambda_r = 0.559 \times 10^{-2}k_{\alpha 2} - 0.725 \times 10^{-3}k_{\alpha 1}^2 - 0.830 \times 10^{-3}k_{h1}k_{\alpha 1} - 2.199 \times 10^{-7}k_{h2} - 1.045 \times 10^{-7}k_{h1}^2 - 0.078c_s$$

$$\begin{aligned} \mathrm{Im}(\Lambda) = \Lambda_i = {} & 0.936 \times 10^{-2}k_{\alpha 2} - 0.119 \times 10^{-2}k_{\alpha 1}^2 - 0.138 \times 10^{-2}k_{h1}k_{\alpha 1} - 0.798 \times 10^{-7}k_{h2} - 0.380 \\ & \times 10^{-7}k_{h1}^2 - 0.137c_s \end{aligned} \tag{37}$$

and Re and Im stand for the real and imaginary parts, respectively.

Letting $\eta = \frac{1}{2}r\exp(\mathrm{i}\theta)$ and separating the real and imaginary parts in Eq. (36), we obtain the following alternate real-valued normal form of the Hopf bifurcation:

$$\dot{r} = \beta_r r + \tfrac{1}{4}\Lambda_r r^3 \tag{38}$$

$$\dot{\theta} = \beta_i + \tfrac{1}{4}\Lambda_i r^2 \tag{39}$$

where r is the amplitude and $\dot{\theta}$ is the shift in the frequency of the periodic solution that is created due to Hopf bifurcation. We note that, because the r component is independent of θ, the problem is reduced to studying the stability of the fixed points of the one-dimensional system (38). Assuming that $\Lambda_r \neq 0$, Eq. (38) admits three equilibrium solutions, namely

$$r = 0, \quad r = \pm\sqrt{\frac{-4\beta_r}{\Lambda_r}} \tag{40}$$

The trivial fixed point of Eq. (38) corresponds to the fixed point (0,0) of Eq. (7), and a nontrivial fixed point (i.e, $r \neq 0$) of Eq. (38) corresponds to a periodic solution of Eq. (7). The origin is asymptotically stable for $\beta_r < 0$, unstable for $\beta_r > 0$, unstable for $\beta_r = 0$ and $\Lambda_r > 0$, and asymptotically stable for $\beta_r = 0$ and $\Lambda_r < 0$. On the other hand, the nontrivial fixed points exist when $-\beta_r\Lambda_r > 0$. They are stable for $\beta_r > 0$ and $\Lambda_r < 0$ (supercritical Hopf bifurcation) and unstable for $\beta_r < 0$ and $\Lambda_r > 0$

(subcritical Hopf bifurcation). We note that a stable nontrivial fixed point of Eq. (38) corresponds to a stable periodic solution of Eq. (7). Likewise, an unstable nontrivial fixed point of Eq. (38) corresponds to an unstable periodic solution of Eq. (7).

4.1. Case study

In order to check the accuracy of the analytical formulation given by the normal form in predicting the amplitude of LCO, we consider the case in which structural nonlinearity is applied only in the pitch degree of freedom; that is, $k_{h1}=0$, $k_{h2}=0$, $c_s=0$, $k_{\alpha 1}=29.996\,\mathrm{N\,m}$, and $k_{\alpha 2}=67.685\,\mathrm{N\,m}$. This configuration corresponds to a supercritical instability ($\Lambda_r<0$). To determine the amplitude of LCO associated with the pitch and plunge motions from the normal form, we consider the first-order solution given by Eq. (29). The amplitude of plunge and pitch LCO, A_h and A_α, respectively, are given by

$$A_h = r\sqrt{\mathbf{p1}_r^2+\mathbf{p1}_i^2}$$

$$A_\alpha = r\sqrt{\mathbf{p2}_r^2+\mathbf{p2}_i^2} \tag{41}$$

where $\mathbf{pj}_r$ and $\mathbf{pj}_i$ denote the real and imaginary part of the j th component of the vector $\mathbf{p}$, respectively. In Figs. 7(a) and (b), we plot the LCO amplitudes for both pitch and plunge motions obtained by integrating the original system and those predicted from the normal form. The results show a good agreement in the amplitudes of LCO near the bifurcation.

To see the effect of the linear and nonlinear parameters on the system's behavior, we vary $k_{\alpha 0}$ by 10 percent, $k_{\alpha 1}$ and $k_{\alpha 2}$ by 20 percent and plot in Fig. 8 variations of the LCO amplitudes with the freestream velocity for the two configurations. Clearly, the effect of combined uncertainties in the linear and nonlinear parameters may cause the flutter to occur at speeds that are much lower than the flutter speed predicted by the linear model. Furthermore, they can cause a switch from a supercritical instability to a subcritical one.

4.2. Sensitivity analysis

The effects of the structural stiffness and aerodynamic nonlinearity on the system behavior can be determined from the normal form. In fact, by setting β_r equal to zero, we can easily assess sensitivity of the flutter speed to variations in the structural pitch and plunge stiffness. For the specific values of the airfoil geometry [10], we observe that

1. Variations in $k_{\alpha 0}$ and k_{h0} have opposite effects on the flutter speed as determined from the signs in Eq. (37).
2. The effect of variations of k_{h0} is twice that of $k_{\alpha 0}$ as determined from the slopes in Figs. 9(a) and (b).
3. The perturbation analysis is valid for small fluctuations of $k_{h\,0}$ and $k_{\alpha 0}$ around their mean values, (see Figs. 9(a) and (b)).

As shown in Eq. (37), the different nonlinearities may be favorable or unfavorable. For example, for the specific values of the system parameters [10], we conclude that

1. In absence of the plunge stiffness nonlinearity, the pitch stiffness nonlinearity, even in the presence of the aerodynamic nonlinearity, may lead to large-amplitude LCO when transitioning through the Hopf bifurcation and also induce LCO even below the nominal flutter velocity if the disturbances to the system are sufficiently large (subcritical Hopf bifurcation).

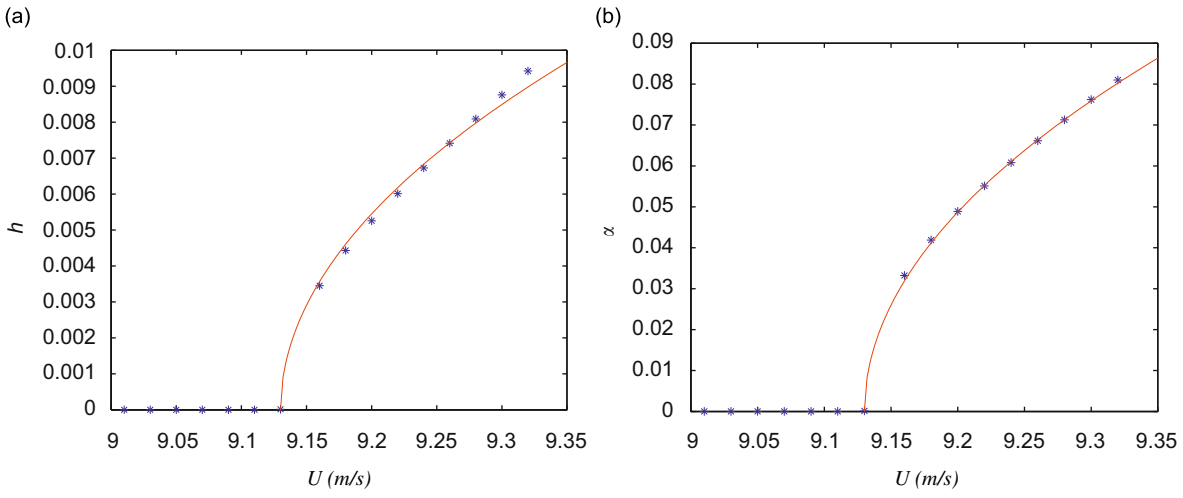

Fig. 7. LCO amplitudes of plunge and pitch motions: -, analytical prediction, ∗, numerical integration. (a) Plunge motion and (b) pitch motion.

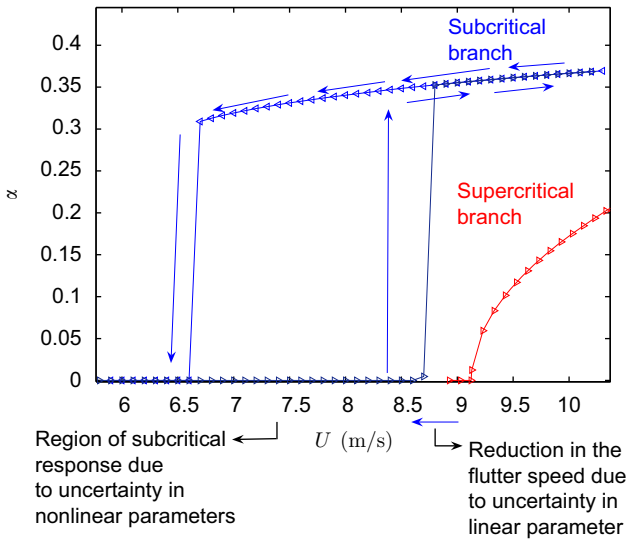

Fig. 8. LCO amplitudes of pitch motion. Arrows show path of system response that may occur due to the effect of combined uncertainties in linear and nonlinear parameters: (→) increasing, (←) decreasing.

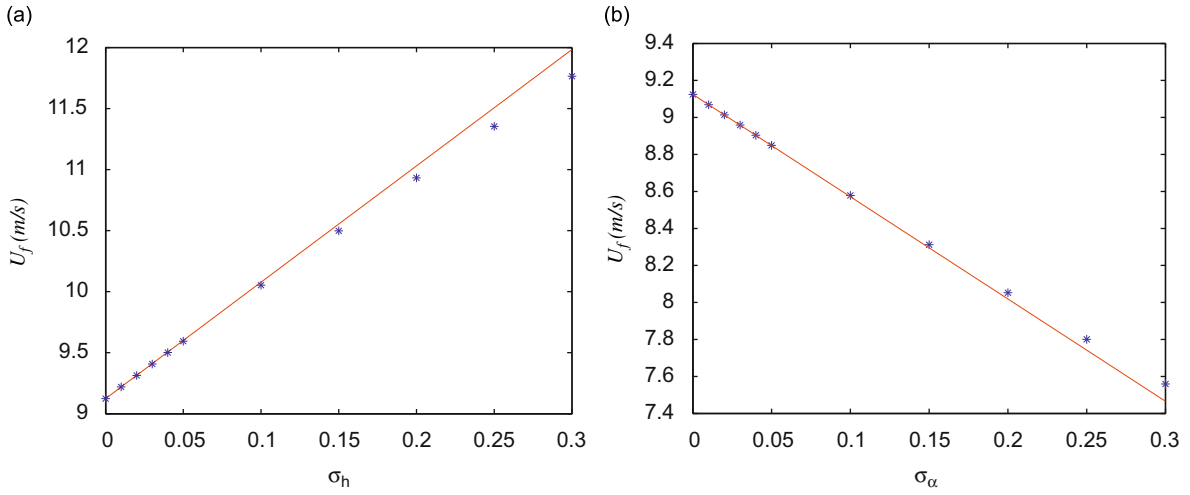

Fig. 9. Sensitivity of the flutter speed to variations in the structural stiffness. The solid line represents the flutter speed obtained from the perturbation analysis. The stars represent the exact flutter speed. (a) Plunge structural stiffness and (b) pitch structural stiffness.

2. The nonlinearity in the plunge stiffness (i.e., $k_{h1} \neq 0$ and $k_{h2} \neq 0$) is favorable in the sense that it inhibits the occurrence of LCO below the flutter boundary and limits the exponentially growing oscillations predicted by the linear model to a periodic response whose amplitude increases slowly with increasing freestream velocity (supercritical Hopf bifurcation).
3. Variations in the different system parameters, such as linear and nonlinear stiffness, can lead to a subcritical instability even if the deterministic problem does not exhibit that behavior.

These observations are based on the assumptions that all springs are of the hardening type. For softening springs, the analysis would yield other responses.

To gain more insight into the combined effect of the cubic and quadratic pitch stiffness coefficients $k_{\alpha 1}$ and $k_{\alpha 2}$ on the type of instability, we generate a contour plot showing variations of Λ_r with $k_{\alpha 1}$ and $k_{\alpha 2}$ (see Fig. 10). We note that only the pitch stiffness nonlinearity is considered; that is, $k_{h1}=0$, $k_{h2}=0$, $c_s=0$. This plot reveals the effect of the pitch stiffness nonlinearity on the type of instability as well as the amplitude of LCO using Eqs. (40) and (41).

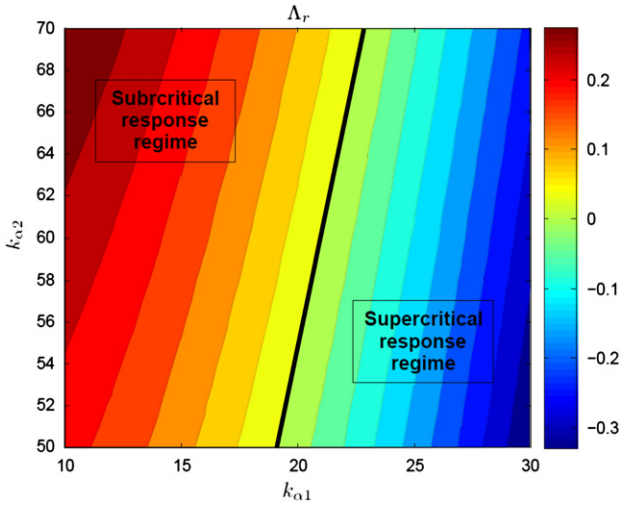

Fig. 10. Variation of Λ_r with $k_{\alpha 1}$ and $k_{\alpha 2}$: effect of the pitch stiffness nonlinearity on the type of instability.

5. Conclusions

In this work, we follow two approaches to determine the effects of variations in the linear and nonlinear plunge and pitch stiffness coefficients of an aeroelastic system on its stability near the bifurcation. The first approach is based on implementing the intrusive PCE on the governing equations, yielding a set of nonlinear coupled ordinary-differential equations that are numerically solved. The results show that this technique is capable of determining sensitivity of the flutter speed to variations in the linear pitch stiffness coefficient. On the other hand, it fails to predict changes in the type of the instability associated with randomness in the cubic stiffness coefficient. The second approach is based on using the normal form to characterize the dynamic instability. Furthermore, the results show that this form can be used to effectively perform sensitivity analysis of the system's response to variations in its parameters.

Although the normal form here has been derived for a low-order system, A.H. Nayfeh [17] presents details on its implementation in higher-dimensional problems. Alternatively, one may apply the normal form to derived phenomenological or physical-based reduced-order models that accurately describe the phenomenon of interest as identified from higher-order representations [18–20]. These models are derived by exploiting a specific phenomenon [21], modeling the nonlinear responses [22], or determining the form of parameters to be identified [23].

Acknowledgments

M. Ghommem is grateful for support from the Virginia Tech Institute for Critical Technology and Applied Science (ICTAS) Doctoral Scholars Program.

References

[1] B.H.K. Lee, L.Y. Jiang, Y.S. Wong, Flutter of an airfoil with a cubic restoring force, *Journal of Fluids and Structures* 13 (1999) 75–101.
[2] C.C. Chabalko, M.R. Hajj, D.T. Mook, W.A. Silva, Characterization of the lco response behaviors of the nata model, *Proceedings of the 47th AIAA/ASME/ASCE/AHS/ASC Structures, Structural Dynamics, and Materials Conference*, AIAA Paper No. 2006-1852, 2006.
[3] P.S. Beran, C.L. Pettit, D.R. Millman, Uncertainty quantification of limit-cycle oscillations, *Journal of Computational Physics* 216 (2006) 217–247.
[4] C. Wu, H. Zhang, T. Fang, Flutter analysis of an airfoil with bounded random parameters in incompressible flow via Gegenbauer polynomial approximation, *Aerospace Science and Technology* 11 (2007) 518–526.
[5] D.R. Millman, P.I. King, P.S. Beran, Airfoil pitch-and-plunge bifurcation behavior with fourier chaos expansions, *Journal of Aircraft* 42 (2005) 376–384.
[6] M.S. Allen, J.A. Camberos, Comparison of uncertainty propagation/response surface techniques for two aeroelastic systems, *Proceedings of the 50th AIAA/ASME/ASCE/AHS/ASC Structures, Structural Dynamics, and Materials Conference*. AIAA Paper No. 2009-2269, 2009.
[7] J.A.S. Witteveen,Uncertainty Quantification Methods for Flow and Fluid-Structure Interaction Simulations. PhD Thesis, Delft University of Technology, The Netherlands, 2008.
[8] J.-C. Chassaing, D. Lucor, Stochastic aeroelastic analysis of a pitching and plunging airfoil in an incompressible flow, *International Forum on Aeroelasticity and Structural Dynamics*, 2009.
[9] H.C. Gilliatt, T.W. Strganac, A.J. Kurdila, An investigation of internal resonance in aeroelastic systems, *Nonlinear Dynamics* 31 (2003) 1–22.
[10] T.W. Strganac, J.J. Ko, D.E. Thompson, Identification and control of limit cycle oscillations in aeroelastic systems, *Proceedings of the 40th AIAA/ASME/ASCE/AHS/ASC Structures, Structural Dynamics, and Materials Conference and Exhibit*, AIAA Paper No. 99-1463, 1999.
[11] H.N. Najm, Uncertainty quantification and polynomial chaos techniques in computational fluid dynamics, *Annual Review of Fluid Mechanics* 41 (2009) 35–52.
[12] D. Xiu, G.E. Karniadakis, Modeling uncertainty in flow simulations via generalized polynomial chaos, *Journal of Computational Physics* 187 (2003) 137–167.

[13] R. Ghanem, P.D. Spanos, *Stochastic Finite Elements: A Spectral Approach*, Dover Publications, Inc., New York, 2003.
[14] C.L. Pettit, P.S. Beran, Spectral and multiresolution wiener expansions of oscillatory stochastic processes, *Journal of Sound and Vibration* 294 (2006) 752–779.
[15] A.H. Nayfeh, B. Balachandran, *Applied Nonlinear Dynamics*, Wiley Series in Nonlinear Science, NY, 1994.
[16] A.H. Nayfeh, *Introduction to Perturbation Techniques*, Wiley Series in Nonlinear Science, NY, 1993.
[17] A.H. Nayfeh, *Method of Normal Forms*, Wiley Series in Nonlinear Science, NY, 1993.
[18] A.H. Nayfeh, W. Lacarbonara, On the discretization of spatially continuous systems with quadratic and cubic nonlinearities, *JSME International Journal* 41 (1998) 2–23.
[19] C.-M. Chin, A.H. Nayfeh, H.N. Arafat, W. Lacarbonara, Multimode interactions in suspended cables, *Journal of Vibration and Control* 8 (2002) 337–387.
[20] C.-M. Chin, A.H. Nayfeh, A second-order approximation of multi-modal interactions in externally excited circular cylindrical shells, *Nonlinear Dynamics* 26 (2001) 45–66.
[21] C. Chabalko, M.R. Hajj, W. Silva, Interrogative testing for nonlinear identification of aeroelastic systems, *AIAA Journal* 46 (2008) 2657–2658.
[22] A.H. Nayfeh, M.R. Hajj, S.A. Nayfeh, P.S. Beran, A reduced-order model for lco dependence on mach number in f16 flight tests, *Proceedings of the 49th AIAA/ASME/ASCE/AHS/ASC Structures, Structural Dynamics, and Materials Conference*, AIAA Paper No. 2008-1755, 2008.
[23] A.H. Nayfeh, F. Owis, M.R. Hajj, A model for the coupled lift and drag on a circular cylinder, *Proceedings of the ASME 19th Biennial Conference on Mechanical Vibrations and Noise*. DETC2003/VIB-48455, 2003.